Large Electropositive Cations as Surfactants for the Growth of Polar Epitaxial Films

by

Alfred Ka Chun Cheung

B.Sc., The University of British Columbia, 2013

A THESIS SUBMITTED IN PARTIAL FULFILLMENT OF
THE REQUIREMENTS FOR THE DEGREE OF

MASTER OF SCIENCE

in

The Faculty of Graduate and Postdoctoral Studies

(Physics)

THE UNIVERSITY OF BRITISH COLUMBIA

(Vancouver)

August 2015

Abstract

Using density functional theory (DFT) we demonstrate that the adsorption of large cations such as potassium or cesium facilitates the epitaxial growth of polar $LaAlO_3$ (LAO) on $SrTiO_3$ (STO). The low ionization potential of K favors efficient electron transfer to the STO conduction band and results in a 2D electron gas which exactly compensates for the diverging potential with increasing layer thickness. For large cations like K or Cs, DFT total energy considerations show that they remain adsorbed on the LAO surface and do not enter substitutionally into LAO. These results suggest a novel scheme for growing clean LAO/STO interface systems, and polar systems in general, by performing the growth process in the presence of large, low ionization potential alkali metal ions.

Preface

The results of this thesis have been published in Physical Review B as A. K. C. Cheung, I. Elfimov, M. Berciu, and G. A. Sawatzky, Phys. Rev. B **91**, 125405 (2015). The calculations were performed by the author, Alfred Cheung, and the interpretation and analysis of the results were done by Alfred Cheung, Ilya Elfimov, Mona Berciu, and George Sawatzky. All density functional theory calculations were performed using the Vienna *ab initio* simulation package (VASP).

Table of Contents

List of Figures

Acknowledgements

I would like to express my deepest gratitude to my two research supervisors Professors Mona Berciu and George Sawatzky. It is hard to overstate how much I have learned and grown as a young physicist under their guidance these past two years. They are truly amazing scientists and people. I am especially indebted to Mona who first introduced me to the fascinating world of condensed matter physics and gave me my first taste of research way back in my undergraduate days.

I would also like to thank Dr. Ilya Elfimov who often acted as a third research supervisor to me during my degree. I owe all my knowledge and insight of density functional theory to Ilya.

Finally, I would like to thank all my fellow group members. I am particularly grateful for the interesting and useful discussions I've had with Dr. Robert Green and Mirko Möller.

Chapter 1

Introduction

One of the fascinating aspects of the study of transition metal and rare earth oxides is the essentially boundless possibilities for synthesizing new materials with novel properties. Of particular interest are the *perovskite* class of materials which are the focus of this thesis. The perovskites are known to exhibit rich phase diagrams with a myriad of electronic, structural, and magnetic phase transitions. The properties of these materials are highly sensitive to very slight changes in geometrical parameters such as bond lengths and angles. Consequently, changing the identity of the cationic species, which directly affect the lattice structure, can lead to drastic changes in the properties of the perovskite.

As if the potential for discovering novel phases from bulk perovskite materials is not enough, the advent of *epitaxial* layer-by-layer growth of materials through molecular beam epitaxy (MBE) and pulsed laser deposition (PLD) has further extended the horizon in this field. Epitaxial growth methods have allowed for the growth of materials that otherwise do not exist in bulk form. Furthermore, stress and strain, which affect bond angles and bond lengths, can be applied to epitaxially grown materials by controlling the identity of the substrate. Finally and most importantly for the topic of this thesis, it is found that at the interface of two oxide materials engineered by epitaxial growth, novel properties emerge that are often completely different from the bulk properties of the constituent materials. This leads to the new frontier of *oxide heterostructures*.

One of the most famous examples in recent years of how the interface can differ completely from the bulk is the case of polar $LaAlO_3$ (LAO) epitaxially grown on top of a non-polar $SrTiO_3$ (STO) substrate. LAO and STO are both large band gap insulators in their bulk forms. However, it was discovered by Ohtomo and Hwang in 2004 that when polar LAO is grown epitaxially on top of STO, a high mobility quasi-2 dimensional electron gas (q-2DEG) is found at the n-type (TiO_2/LaO) interface [1]. Since the discovery of this q-2DEG, enormous efforts have been made to understand its origins and its relation to the polar, crystallographic orientation induced electric potential which diverges with the LAO film thickness – the

so-called "polar catastrophe" [2–4]. Indeed, while the mechanism for the formation of this q-2DEG is still highly controversial, what is agreed upon is how intriguing this system is for both basic and applied science. From a more fundamental point of view, superconductivity and magnetism and their coexistence have been found in this q-2DEG [5–7]. From a more applications oriented perspective, it has been found that the conductivity of this system can be controlled through external electric potentials and by varying the LAO film thickness [8].

Before the LAO/STO interface system can be understood and utilized in any application, clean growth must first be achieved. The importance of having a controlled scheme for growing clean interfaces is reflected by how samples grown by different groups can exhibit very different properties [9]. The daunting challenge of achieving clean growth is a natural outcome of the polar nature of the system: there are simply too many ways in which the system can compensate for the polar diverging potential, and each of these changes the properties of the resulting epitaxial film. Thus, the polar catastrophe is somewhat of a mixed blessing – without it, there would be no q-2DEG at all and this system would not be interesting; with it, we lose control over the quality of the interface.

In this thesis, we propose a novel solution for this challenge. Our proposal is to purposely introduce a minute concentration of potassium atoms into the epitaxial growth chamber, which are then adsorbed onto the AlO_2 surface as a surfactant. Our reasoning is that potassium, being an alkali metal, very readily gives up an electron. Thus, when it is adsorbed, electrons from the potassium surfactant layer can be donated to the interface at an energy cost significantly lower than other competing compensation mechanisms. Using density functional theory (DFT) calculations, we show that this is this is indeed the case. Furthermore, we also show that due to the large size of potassium ions, substitution into the LAO film is highly unlikely, a necessary property for an effective surfactant.

The thesis is organized as follows. In Chapter 2, we give an overview of the background of the LAO/STO interface system and the concept of polar catastrophe. We also motivate our proposal for clean epitaxial growth by the use of large electropositive cations as surfactants. In Chapter 3, we provide a review of density functional theory. We then present our findings in Chapter 4. Finally, we conclude in Chapter 5 with a summary and further discussions.

Chapter 2

Background

2.1 The polar catastrophe

Because the polar catastrophe is essentially an electrostatic effect that arises due to the charge distribution and spatial termination of a crystal, to understand its role in the LAO/STO interface system we must first consider separately the crystal structure of LAO and STO. As stated in the previous chapter, both LAO and STO crystallize in a simple ABO_3 (A and B are cations) perovskite structure consisting of alternating layers of AO and BO_2. The idealized simple cubic unit cell is shown in Fig. 2.1.

For $SrTiO_3$, the A cation is Sr^{2+} and the B cation is Ti^{4+}. The structure thus consists of alternating *charge neutral* SrO and TiO_2 planes (oxygen has a formal oxidation number of 2+). For $LaAlO_3$ however, the situation is different with the A cation being La^{3+} and the B cation Al^{3+}. In this case, the LaO plane has a net charge of $+1$ and the AlO_2 plane has a net charge of -1 per unit cell. Hence in LAO, we obtain a system consisting of alternating, oppositely charged layers.

For LAO, what electric potential profile is obtained within such a system of alternating charged layers? To understand this at a basic conceptual level, let us make a further simplification and assume that each charged layer is a uniformly charged sheet with charge density $\pm\sigma$. From elementary electrostatics, we know that each sheet produces a constant electric field $(\sigma/2\epsilon)\hat{n}$ where ϵ is the dielectric constant of the medium, and $\hat{n}$ is the unit vector normal to and pointing away from the sheet.

With this setup, we can easily deduce the electric field as a function of the position z normal to the charged sheets. For a system of six layers, this is shown in Fig. 2.2a. The electric field alternates between 0 and $+(\sigma/\epsilon)\hat{z}$ in the regions between the sheets. To get the electric potential as a function of z, we simply integrate the electric field. The result is shown in Fig. 2.2b. A non-zero potential drop exists between the top and bottom layers. *Furthermore, this potential drop increases as more layers are added.* Taking this example back to the case of LAO, it can be shown that over nanometer length scales, this potential drop is of the order of tens of electron volts.

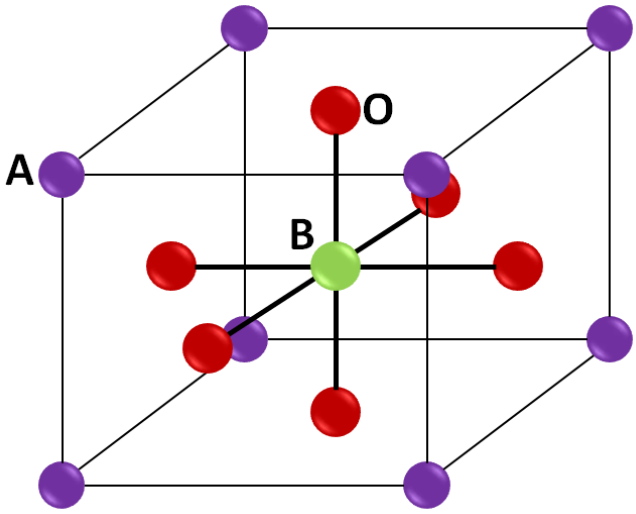

Figure 2.1: The simple cubic unit cell of ABO_3 perovskite. The structure consists of alternating AO and BO_2 layers.

Such a system is clearly unstable, and it must change in some way to remove this diverging potential. This highly unstable build up of a potential difference over microscopic length scales, essentially due to crystallographic properties, is known as the polar catastrophe and it is expected to play a critical role in systems such as (001)-terminated LAO.

2.2 Compensation mechanisms

2.2.1 Electronic reconstruction

If a system is strongly polar, what are the available mechanisms for the system to remove the electric potential build up? One option, proposed by Ohtomo and Hwang to explain the existence of the q-2DEG at the LAO/STO interface, is *electronic reconstruction* [3, 4, 10]. Consider an n-type LAO/STO interface, again in the simplified picture of viewing each charged layer as a uniformly charged sheet. In the non-compensated system with alternating charge +1/-1 layers, we saw that the potential difference grows as the LAO thickness increases. However, what happens if half an electron per unit cell is transferred from the top AlO_2 layer to the interface?

In this case, the top AlO_2 layer is left with a net charge of +1/2 per unit

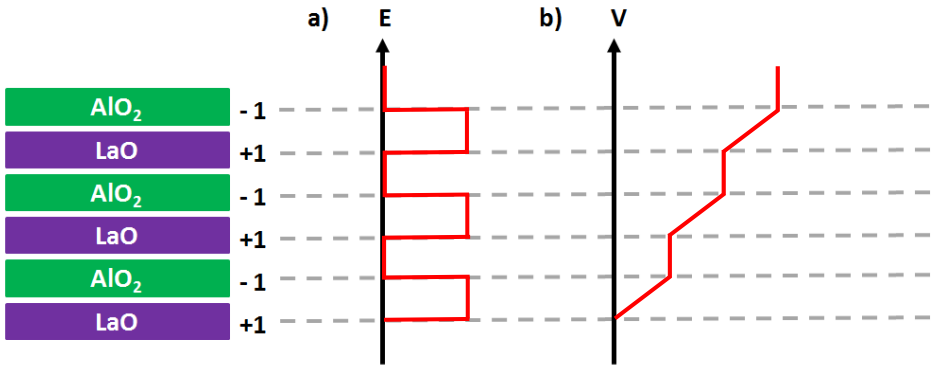

Figure 2.2: Simplified electrostatics view of the polar catastrophe in LAO. (a) The electric field is sketched as a function of the position along the polar direction, normal to the layers. The field alternates between 0 and a non-zero value. When integrated to get the electric potential, a net potential difference exists across the film which increases with the film thickness, as shown in (b). The divergence in potential as film thickness is increased is known as the polar catastrophe. Its high energetic cost forces the system to reconstruct in one way or another in order to negate the potential build up. Figure adapted from Ref. [3].

cell, while the interface between LAO and STO acquires a net charge of -1/2 per unit cell. By the same elementary electrostatics analysis done earlier, it can be shown that the electric field now alternates between $+(\sigma/2\epsilon)\hat{z}$ and $-(\sigma/2\epsilon)\hat{z}$ in the regions between the sheets, as shown in Fig. 2.3a. Integrating to get the electric potential, we find that it *no longer diverges with film thickness* as shown in Fig. 2.3b. In this way, the polar catastrophe has been negated. Moreover, in this theory, the -1/2 electrons per unit cell donated to the interface forms the q-2DEG seen in experiments.

The electronic reconstruction picture is appealing in its simplicity. Unfortunately, it fails to explain a few key experimental observations. Firstly, the energy cost associated with the transfer of 1/2 an electron per unit cell, essentially the band gap between the valence band of LAO and the conduction band of STO, predicts the onset of electronic reconstruction to occur at a LAO thickness of 1-2 layers (the thickness dependent potential build up must exceed this band gap for a Zener breakdown to occur and the electrons to be transferred). However, the critical thickness is experimentally measured to be at 4 unit layers [4]. Secondly, the electron transfer mechanism

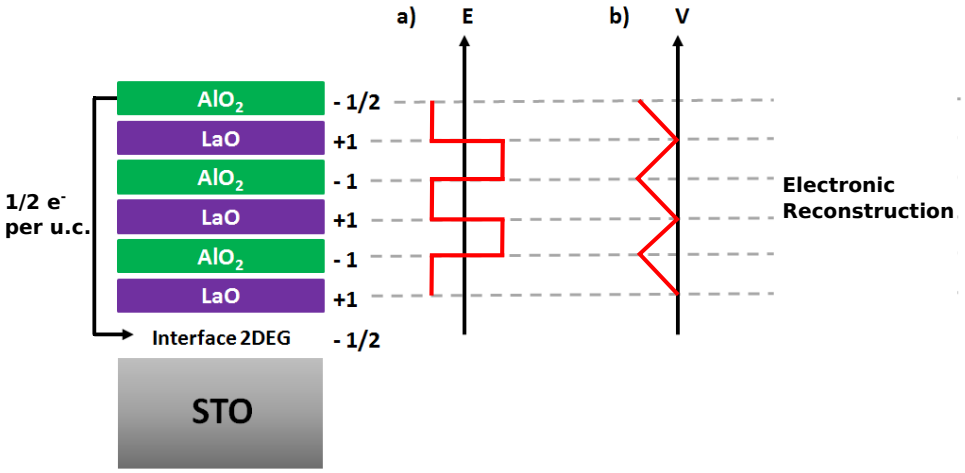

Figure 2.3: Simplified electrostatics view of electronic reconstruction as a compensation mechanism for the polar catastrophe at an n-type LAO/STO heterojunction. In this simple picture, half an electron per unit cell is transferred from the top AlO_2 layer to the interface. This results in the electric field as a function of the normal position as shown in (a). The electric field alternates between opposite direction. The electric potential obtained when the field is integrated is shown in (b). In contrast to the unreconstructed system of Fig. 2.2, there is no longer a net potential difference across the LAO film. In this theory, the transferred electrons enter into the empty $3d$ orbitals of the interface TiO_2 layer, forming the q-2DEG observed in experiment. Figure adapted from Ref. [3].

predicts that the number of electrons transferred should increase gradually from zero at the critical thickness. In contrast, experimentally, the carrier density at the interface is observed to jump to a non-zero value at the critical thickness and then remain constant as the LAO thickness is further increased [4]. Finally, electronic reconstruction predicts the existence of a conducting hole gas at the top AlO_2 surface in addition to the q-2DEG at the interface. No such surface conductivity has been observed.

2.2.2 Compensation by surface oxygen vacancies

Clearly, electronic reconstruction cannot be the whole story. Other compensating mechanisms must exist to account for what is observed experimentally. One particularly promising proposal is compensation via the formation of surface oxygen vacancies [6, 8, 12–24]. In this proposal, 1 out of 8 oxygen atom sites are vacant on the top AlO_2 surface. In other words, the surface formula unit is $AlO_{1.75}$ leading to a net charge of $+1/2$. Additionally, the missing O^{2-} anions must have left behind 2 electrons each. These are transferred to the interface and form the q-2DEG. Overall, the top $AlO_{1.75}$ surface acquires an effective net charge of $+1/2$ per unit cell while the interface acquires a net charge of -1/2 per unit cell. Hence, the polar problem is solved and the q-2DEG at the interface is accounted for, as in the electronic reconstruction scenario. A key difference exists in this case however – the oxygen vacancies are immobile on the surface and therefore do not lead to any surface conductivity. This is in agreement with experiment.

Besides accounting for the insulating behaviour of the AlO_2 surface, the surface oxygen vacancy picture also explains the abrupt increase in interface carrier density at the critical thickness and its constant value as more LAO layers are grown. Consider that at thicknesses below the critical thickness, the energy cost for forming a surface oxygen vacancy must be positive (it costs energy to form a lattice vacancy). As the thickness of LAO is increased and the polar electric potential builds up, the energy cost must decrease. Finally, at the critical thickness, the vacancy formation energy becomes negative [24]. Forming an oxygen vacancy now stabilizes the system and surface oxygen vacancies spontaneously form at (in an ideal case) a concentration of 1/8. Once the vacancies have formed and electrons are transferred to the interface, the polar problem no longer exists and increasing the LAO thickness further makes no change. Hence, compensation by surface oxygen vacancies can be said to be a “one-off” process, thereby explaining the abrupt increase in the interface carrier density at the critical thickness and its constant value for higher thicknesses.

2.2.3 Other compensating mechanisms

Although we have discussed in detail only two compensating mechanisms, many credible alternatives have been proposed, each often explaining certain aspects of the experimental observations while failing to rationalize others. For example, Pickett and Pentcheva used DFT calculations to demonstrate that within the LAO film, buckling of the lattice can partially reduce the polar potential [25, 26]. In their proposal, La^{3+} and Al^{3+} cations are displaced relative to the O^{2-} anions. The relative displacement occurs such that internal dipoles are formed which create electric fields opposite in direction to the electric field formed by the overall polar crystal orientation. The net effect is to partially reduce the polar potential build up and increase the critical thickness required for electronic reconstruction to become energetically favourable. Other proposed mechanisms include cation intermixing between STO and LAO at the interface as well as interface defects [11, 12].

Which one of these mechanisms is truly responsible for the compensation of the polar catastrophe and the existence of the q-2DEG? There really is no answer to this question because there is no reason why these compensation mechanisms should be mutually exclusive. Although the issue is still under debate, there is now consensus that compensation of this diverging electric potential (the polar catastrophe) is achieved through a combination of pure electronic reconstruction, interface defects, lattice distortions, and oxygen vacancies. The relative contributions of these mechanisms to removing the polar catastrophe is expected to depend critically on the specific details of the growth conditions. This likely explains why samples grown by different groups can show widely dissimilar properties. The important role played by defects and vacancies [3] also explains why the growth of clean LAO/STO interfaces, necessary for device applications, has proven to be such a challenge.

2.3 Our proposal

In this thesis the main problem we aim to solve can thus be framed as follows: *how can clean epitaxial growth be achieved for the LAO/STO system and more generally with any strongly polar epitaxial film?* From the preceding discussion, we have established that this is basically a question of competing energy costs for various compensation mechanisms. Because no particular compensation mechanism that is available to the system is substantially more energetically efficient compared to the others, they all come into play to varying degrees. The outcome is the lack of control over

sample quality seen in experiments. Therefore, if the growth conditions can be modified such that a particular compensation mechanism becomes much more thermodynamically efficient, then this problem would be solved.

Our proposal to purposely introduce a minute amount of potassium into the growth chamber is based precisely on this principle. We use DFT calculations to show that a coverage of 1/2 K per unit cell of the AlO_2 surface of LAO acts like a surfactant that stabilizes the epitaxial growth of the polar LAO on top of STO. Each K donates an electron to the LAO/STO interface, generating a q-2DEG while keeping the top LAO surface insulating. This compensates for the polar catastrophe for any LAO film thickness, removing the reason for the appearance of defects, vacancies or distortions. Moreover, substitution of the large K ions into the LAO film is unlikely for epitaxial type growth. As a result, after the deposition of half a monolayer of K, the LAO film will grow cleanly under this surfactant.

We emphasize that we use the term *surfactant* as is customary in the crystal growth community [27, 28]: a surfactant facilitates the growth of the film while "floating" on its surface [27–31]. An effective surfactant is energetically most favored on the film's surface [29]; when an adatom (La, Al, and O) arrives onto the surface, the adatom and a surfactant atom (K) exchange positions such that the surfactant re-emerges on the surface and the adatom is buried underneath. The process is then repeated [27–32].

Our proposal is supported by past successes in using surfactants to stabilize crystal surfaces [27–35]. For example, (111)-terminated MnS, otherwise impossible to grow due to the polar problem, was stabilized by adsorption of I^- on its surface [33]. The use of alkali metals as electron donors is also common: K deposition onto $YBa_2Cu_3O_{6+x}$ was used to tune its doping level [36, 37]. Indeed, although we focus in this thesis on LAO/STO, there is no obvious reason for this method to not work for other polar materials. We believe that, in general, the use of low ionization energy surfactants can facilitate the growth of ionic materials with strongly polar orientations.

Chapter 3

Density Functional Theory

We claim that our proposed scheme for clean epitaxial growth should be applicable to the entire class of materials with strongly polar orientations. Nevertheless, because we largely illustrate the physics using the LAO/STO interface system as a specific material example, the theoretical technique we choose must naturally be one of the *ab initio* methods. The best modern technique for such purposes is density functional theory. Hence, we devote this chapter to an overview of the formalism behind DFT. We will aim to only stress the main ideas without delving into rigorous proofs and details.

In the spirit of *ab initio* methods, the goal is to solve for the many-electron wavefunction Ψ which satisfies the Schrödinger equation $\hat{H}\Psi = E\Psi$, given the positions and charges of all the positive nuclei. The general (non-relativistic) electronic Hamiltonian $\hat{H}$ (in atomic units) assumes the following form:

$$\hat{H} = -\frac{1}{2}\sum_{i=1}^{N}\nabla_i^2 + \sum_{i=1}^{N}\sum_{j>i}^{N}\frac{1}{|\mathbf{r}_i - \mathbf{r}_j|} - \sum_{i=1}^{N}\sum_{A=1}^{M}\frac{Z_A}{|\mathbf{r}_i - \mathbf{R}_A|}, \tag{3.1}$$

where N is the total number of electrons, M is the total number of nuclei, $\mathbf{r}_i$ is the position vector of electron i, $\mathbf{R}_A$ is the position vector of of nucleus A, and Z_A is the charge of nucleus A. Note that we have already used the Born-Oppenheimer Approximation in which the positions of the positive nuclei are frozen and they provide only a fixed external potential felt by the electrons. The first term gives the electron kinetic energy, the second term gives the electron-electron repulsion, and the last term gives the external potential from the positive nuclei. *Note that the first two terms are universal to all electron system, while the last term is unique to any given system.*

Solving for $\Psi(\mathbf{r}_1, ..., \mathbf{r}_N)$ is a truly challenging if not impossible task. Students of undergraduate level quantum mechanics know that there is already no analytical solution for $N > 1$. Either approximations must be made, or numerical methods must be employed. For larger N, even numerical efforts become futile as computation times scale exponentially with increasing N. Considering that in condensed matter systems, the number of electrons is of

the order 10^{23}, it is easy to dismiss the entire problem as impossible! At this point, two options are available: (1) instead of working with the full Hamiltonian of Eq. 3.1, simpler effective model Hamiltonians can be derived which are much easier to handle but still capture the essential physics; (2) retain the full Hamiltonian of Eq. 3.1 but reformulate the problem such that it is tractable numerically. It is not inaccurate to claim that much of theoretical condensed matter physics is based on using one of these two approaches to the many-body problem.

3.1 The Hohenberg-Kohn Theorems

In DFT, the second approach is taken. Consider the ground state of a many-body system described by the wavefunction $\Psi_0(\mathbf{r}_1, ..., \mathbf{r}_N)$. The basic idea in DFT is that, instead of working with the wavefunction Ψ_0 with $3N$ degrees of freedom, we can instead work with the ground state electron density $n_0(\mathbf{r})$. Clearly, this is a drastic simplification as we have reduced the degrees of freedom to just 3: x, y, and z! But, can the ground state properties of a system, as properly described by the wavefunction Ψ, really be extracted from only the electron density $n_0(\mathbf{r})$? The answer is yes[1], and it is based on the two Hohenberg-Kohn Theorems derived in 1964 [38].

3.1.1 The First Theorem

The first Hohenberg-Kohn theorem states that $n_0(\mathbf{r})$ uniquely determines the external potential $U(\mathbf{r})$, and hence the Hamiltonian, of a fully-interacting system of electrons in the ground state. The proof is by contradiction. Consider two systems described by Hamiltonians $\hat{H}$ and $\hat{H}'$ with two (different) external potentials $V(\mathbf{r})$ and $V'(\mathbf{r})$. The ground state wavefunctions of these systems are Ψ and Ψ', respectively. Assume for now that these wavefunctions have the same ground state electron density $n(\mathbf{r}) = n'(\mathbf{r}) = n_0(\mathbf{r})$.

Let $E_0 = \langle\Psi|\hat{H}|\Psi\rangle$ be the eigenenergy of state Ψ and $E_0' = \langle\Psi'|\hat{H}'|\Psi'\rangle$ be the eigenenergy of state Ψ'. By the variational principle,

$$E_0 < \langle\Psi'|\hat{H}|\Psi'\rangle, \tag{3.2}$$

[1] One might object that other properties, such as whether a material is insulating or metallic, are also considered "ground state properties", which the formalism here fails to describe. However, strictly speaking, there really are no "ground state properties" other than the ground state electron density and the total energy. Whether a material is insulating/semiconducting or metallic, for example, is determined by the conductivity gap, which is related to electron addition and removal energies, i.e. *excited state* properties.

since the state Ψ' is the ground state of Hamiltonian $\hat{H}'$ and not $\hat{H}$. We can express the right hand side of the inequality in Eq. 3.2 as:

$$\begin{aligned}\langle\Psi'|\hat{H}|\Psi'\rangle &= \langle\Psi'|[\hat{H}-\hat{H}']|\Psi'\rangle + \langle\Psi'|\hat{H}'|\Psi'\rangle \\ &= \langle\Psi'|[V(\mathbf{r})-V'(\mathbf{r})]|\Psi'\rangle + E_0' \\ &= \int d^3\mathbf{r}[V(\mathbf{r})-V'(\mathbf{r})]n(\mathbf{r}) + E_0' \\ &= \int d^3\mathbf{r}[V(\mathbf{r})-V'(\mathbf{r})]n_0(\mathbf{r}) + E_0' \end{aligned} \tag{3.3}$$

Hence, the inequality becomes:

$$E_0 < \int d^3\mathbf{r}[V(\mathbf{r})-V'(\mathbf{r})]n_0(\mathbf{r}) + E_0'. \tag{3.4}$$

We can repeat the same steps with Ψ' as the reference system, i.e. consider $E_0' < \langle\Psi|\hat{H}'|\Psi\rangle$. In this case, we have:

$$\begin{aligned}\langle\Psi|\hat{H}'|\Psi\rangle &= -\int d^3\mathbf{r}[V(\mathbf{r})-V'(\mathbf{r})]n'(\mathbf{r}) + E_0 \\ &= -\int d^3\mathbf{r}[V(\mathbf{r})-V'(\mathbf{r})]n_0(\mathbf{r}) + E_0. \end{aligned} \tag{3.5}$$

This leads to the inequality:

$$E_0' < -\int d^3\mathbf{r}[V(\mathbf{r})-V'(\mathbf{r})]n_0(\mathbf{r}) + E_0. \tag{3.6}$$

Finally, adding the inequalities of Eq. 3.4 and Eq. 3.6, we obtain that $E_0+E_0' < E_0+E_0'$ – a contradiction. Therefore, the assumption $n(\mathbf{r}) = n'(\mathbf{r})$ cannot hold; the ground state electron densities from two different external potentials must be different. In other words, there is a unique Hamiltonian for a given ground state density. The converse statement, that there is a unique ground state density for a given Hamiltonian, is trivial assuming a non-degenerate ground state. Thus, we conclude that there is a *one-to-one correspondence* between $n(\mathbf{r})$ and $\hat{H}$.

3.1.2 The Second Theorem

The second Hohenberg-Kohn Theorem establishes a variational principle in terms of the electron density $n(\mathbf{r})$ and it follows closely from the First

Theorem. From the First Theorem, we know that all the information about the ground state, such as the ground state energy, can be obtained from $n(\mathbf{r})$ in place of $\Psi(\mathbf{r}_1, ..., \mathbf{r}_N)$. This means that there exists a functional $\Psi[n(\mathbf{r})]$ which maps $n(\mathbf{r})$ to the corresponding Ψ. There is also a functional of the ground state density for the ground state energy. This justifies the name of Density Functional Theory.

Denote the functional which maps the ground state electron density $n_0(\mathbf{r})$ to the corresponding ground state energy E_0 as $E[n_0(\mathbf{r})]$ such that $E[n_0(\mathbf{r})] = E_0$. Consider a trial state Ψ_t with a corresponding trial electron density $n_t(\mathbf{r})$. The conventional variational principle in terms of states gives $\langle \Psi_t | \hat{H} | \Psi_t \rangle \geq E_0$. But, again by the First Theorem, instead of working with complicated states and wavefunctions, we can simplify the problem and work instead with the electron density $n(\mathbf{r})$. In terms of electron density, the variational condition becomes: $E[n_t(\mathbf{r})] \geq E_0$. Thus, the Second Theorem is basically a reformulation of the variational principle and tells us that to find the true ground state electron density, we must minimize the energy functional with respect to $n(\mathbf{r})$.

3.2 The Kohn-Sham Method

While the Hohenberg-Kohn Theorems firmly establish the theoretical justification for working with electron densities rather than wavefunctions, they do not offer a practical prescription for the calculation of the ground state electron density. This came in 1965 with the introduction of the Kohn-Sham (KS) Method which provided a clear recipe for the self-consistent determination of the ground state density [39]. The KS method remains the only practical implementation of DFT; as such, while DFT, strictly speaking, refers to the much broader formalism in terms of electron density as described by the Hohenberg-Kohn Theorems, in all modern applications of DFT, it is implicit that the KS method has been applied.

In the Kohn-Sham Method, the key simplification is that instead of working with the full interacting system of electrons, we consider a reference non-interacting system. This reference non-interacting system is chosen such that the ground state electron density is equal to that of the actual system of interacting electrons. Provided that this choice is made, the ground state electron density of the reference system can be easily calculated because the system is non-interacting. The wavefunction takes the form of a Slater determinant obtained from filling up the N lowest energy single-particle orbitals $\psi_i(\mathbf{r})$. The electron density is then given by $n(\mathbf{r}) = \sum_{i=1}^{N} |\psi_i(\mathbf{r})|^2$. Of

course, the question now is how can a suitable non-interacting reference system be chosen? The answer is that we do not know how to do this exactly, but we can group all the unknown parts into a term of the non-interacting reference Hamiltonian called the exchange-correlation energy.

Consider the total energy functional $E[n(\mathbf{r})]$ consisting of contributions from kinetic energy $T[n(\mathbf{r})]$, the electron-electron interaction $U_{ee}(\mathbf{r})$, and the external potential $V_{ext}[n(\mathbf{r})] = \int V(\mathbf{r})n(\mathbf{r})d^3\mathbf{r}$:

$$E[n(\mathbf{r})] = T[n(\mathbf{r})] + U_{ee}[n(\mathbf{r})] + \int V(\mathbf{r})n(\mathbf{r})d^3\mathbf{r}. \tag{3.7}$$

Let $T_s[n(\mathbf{r})]$ be the kinetic energy of the reference system. It is in general not equal to the kinetic energy of the original interacting system. We can express the true kinetic energy as the sum of $T_s[n(\mathbf{r})]$ and the difference in the reference and true kinetic energies, denoted here as $\Delta T[n(\mathbf{r})]$:

$$T[n(\mathbf{r})] = T_s[n(\mathbf{r})] + \Delta T[n(\mathbf{r})]. \tag{3.8}$$

The electron-electron interaction term can also be divided into a classical Hartree term and a non-classical exchange term $U_{ex}[n(\mathbf{r})]$:

$$U_{ee}[n(\mathbf{r})] = \frac{1}{2}\int \frac{n(\mathbf{r})n(\mathbf{r}')}{|\mathbf{r}-\mathbf{r}'|}d^3\mathbf{r}d^3\mathbf{r}' + U_{ex}[n(\mathbf{r})]. \tag{3.9}$$

Applying Eq. 3.8 and Eq. 3.9 to Eq. 3.7, we obtain:

$$\begin{aligned} E[n(\mathbf{r})] =& T_s[n(\mathbf{r})] + \Delta T[n(\mathbf{r})] \\ &+ \frac{1}{2}\int \frac{n(\mathbf{r})n(\mathbf{r}')}{|\mathbf{r}-\mathbf{r}'|}d^3\mathbf{r}d^3\mathbf{r}' + U_{ex}[n(\mathbf{r})] \\ &+ \int V(\mathbf{r})n(\mathbf{r})d^3\mathbf{r}. \end{aligned} \tag{3.10}$$

Observe that the only two functionals which we do not know the form of are $\Delta T[n(\mathbf{r})]$, the "correlation energy", and $U_{ex}[n(\mathbf{r})]$, the exchange energy. We group these two unknown functionals together into a single unknown functional $E_{xc}[n(\mathbf{r})]$ – the famous *exchange-correlation energy*. Hence, Eq. 3.10 becomes:

$$E[n(\mathbf{r})] = T_s[n(\mathbf{r})] + \frac{1}{2}\int \frac{n(\mathbf{r})n(\mathbf{r}')}{|\mathbf{r}-\mathbf{r}'|}d^3\mathbf{r}d^3\mathbf{r}' + \int V(\mathbf{r})n(\mathbf{r})d^3\mathbf{r} + E_{xc}[n(\mathbf{r})]. \tag{3.11}$$

We have now succeeded in expressing the total energy functional of the original interacting system in terms of the kinetic energy of the reference

non-interacting system, $T_s[n(\mathbf{r})]$ and the three other terms which we can identify as coming from the effective single-particle potential of the reference system. The form of this effective potential $V_{eff}[n(\mathbf{r})]$ is given by taking the functional derivative of these three terms with respect to $n(\mathbf{r})$. This yields

$$V_{eff}[n(\mathbf{r})] = V(\mathbf{r}) + \int \frac{n(\mathbf{r}')}{|\mathbf{r} - \mathbf{r}'|} d^3\mathbf{r}' + V_{xc}[n(\mathbf{r})], \tag{3.12}$$

where $V_{xc}[n(\mathbf{r})]$ is defined to be $\frac{\delta E_{xc}[n(\mathbf{r})]}{\delta n(\mathbf{r})}$.

Eq. 3.12 represents the single-particle potential that the electrons in the reference non-interacting system experience. *By construction, the ground state electron density of this reference system is the same as that of the original interacting system.* Therefore, *assuming that the form of* $V_{xc}[n(\mathbf{r})]$ *is known*, we now have a self-consistent recipe for the calculation of the ground state density $n(\mathbf{r})$ of the original interacting system:

1. Choose an initial guess for $n(\mathbf{r})$.
2. Construct the effective single-particle potential $V_{eff}[n(\mathbf{r})] = V(\mathbf{r}) + \int \frac{n(\mathbf{r}')}{|\mathbf{r}-\mathbf{r}'|} d^3\mathbf{r}' + V_{xc}[n(\mathbf{r})]$ for the reference non-interacting system.
3. Solve for the ground state of the reference system. The solution is a Slater determinant formed by occupying the N lowest energy single-particle eigenstates $\psi_i(\mathbf{r})$.
4. Recalculate a new $n(\mathbf{r})$ by taking $n(\mathbf{r}) = \sum_{i=1}^{N} |\psi_i(\mathbf{r})|^2$ and repeat steps until convergence of $E[n(\mathbf{r})]$.

The formalism outlined above was based on static positions of the nuclei (the Born-Oppenheimer Approximation). The formalism can be extended to allow for structural relaxation. This is done by first assuming a fixed nuclei configuration and calculating the *electronic* ground state via the recipe above. Next, the net forces on all the nuclei are determined by using the Hellmann-Feynman Theorem. Based on these forces, the nuclei positions are updated and this process if repeated until the forces on all nuclei are below a certain threshold value.

Of course, one major issue remains: we do not know the form of the exchange-correlation energy functional! Various approximations have been made for its form. Much of ongoing theoretical work on the DFT formalism is focused on finding better forms for V_{xc}. While this is a difficult task, the good news is that the exchange-correlation energy is a universal functional that applies to all interacting electron systems: the positions of the positive nuclei do not affect it.

3.2.1 Approximating the exchange-correlation functional

The most important approximation to the exchange-correlation functional is the Local Density Approximation (LDA). In addition to being widely used in its own right, LDA is also the starting point on which many other improvements are based. In LDA, $V_{xc}[n(\mathbf{r})]$ is assumed to take the form:

$$V_{xc}[n(\mathbf{r})] = \int d^3\mathbf{r} n(\mathbf{r}) \epsilon_{xc}(n(\mathbf{r})). \tag{3.13}$$

That is, it is a function only of the local electron densities at each point. An approximation to the function $\epsilon_{xc}(n)$ can be computed numerically for a uniform electron gas [40]. This form is then applied to general systems when $n(\mathbf{r})$ is not uniform. Consequently, LDA works very well for systems with electron densities that vary slowly in space.

The generalized gradient approximation (GGA) is another popular approximation. In GGA, $V_{xc}[n(\mathbf{r})]$ is allowed to depend not only on the local electron densities, but also on the local gradient of the electron density, $\nabla n(\mathbf{r})$ [41]:

$$V_{xc}[n(\mathbf{r})] = \int d^3\mathbf{r} f(n(\mathbf{r}), \nabla n(\mathbf{r})). \tag{3.14}$$

The GGA tends to allow for stronger spatial variation in the electron density. The difficulty with using GGA, however, is that unlike in LDA there is no reference system such as the uniform electron gas which can be used to determine $f(n(\mathbf{r}), \nabla n(\mathbf{r}))$. Thus, various forms of GGA exist. The most widely used one used in solid state physics is the Perdew-Burke-Ernzerhof (PBE) functional [41]. The advantage of the PBE functional is that it depends only on fundamental constants – there are no parameters that must be fitted according to the system being modeled.

3.3 Application to periodic systems

So far, we have presented DFT and the KS Method in a general form suitable for application to any system of interacting electrons and nuclei. Indeed, DFT is used extensively for the study of molecular systems in chemistry, in addition to its traditional applications to crystalline systems in solid state physics. However, since we are concerned here with periodic systems, in this section we will mention some of the important aspects of applying DFT to periodic structures.

As usual for periodic systems, due to the discrete translational symmetry of the lattice, we work within a Brillouin zone defined by the crystal

structure, and crystal momentum $\mathbf{k}$ is a good quantum number. Hence, the single-particle eigenstates of the KS Hamiltonian take the form of Bloch functions labeled by $\mathbf{k}$ and a band index n:

$$\psi_{n\mathbf{k}}(\mathbf{r}) = u_{n\mathbf{k}}(\mathbf{r})e^{i\mathbf{k}\cdot\mathbf{r}}, \tag{3.15}$$

where $u_{n\mathbf{k}}(\mathbf{r})$ is a function with the same periodicity as the lattice. The energies $E_{n\mathbf{k}}$ of these eigenstates *of the Kohn-Sham reference system* define a band structure, which can be summed over to obtain a density of states $\rho(E) = \sum_{n\mathbf{k}} \delta(E - E_{n\mathbf{k}})$. A very important point is that the band structure and density of states obtained do not actually represent the system of interacting electrons! They only describe the electronic structure of the non-interacting Kohn-Sham reference system. The only property of the reference system which does have physical meaning is the ground state electron density. Nevertheless, in DFT, the KS band structure and density of states are often interpreted as describing the electronic structure of the original system in some way. In this work, we will also use this interpretation of the KS density of states.

3.4 Plane wave basis and the motivation for pseudopotentials

The choice of the basis set is also a significant part of applying DFT efficiently. Whereas for isolated molecular systems, it is natural to adopt atomic orbitals centred about each atom as the basis set, for periodic systems, the natural choice is plane waves $e^{i\mathbf{p}\cdot\mathbf{r}}$. Plane waves can be chosen to have arbitrarily high energies (frequencies). Therefore, it is necessary to pick a cutoff energy and only keep in the basis plane waves with energies less than this cutoff. The higher the cutoff, the more complete the basis, and the more accurate the results, at the cost of longer computation times.

One challenge of working with a plane wave basis comes from the shape of the attractive Coulombic potential in regions close to a nucleus. In these regions, the potential goes to very negative values, which in turn means that the eigenfunctions oscillate very rapidly in space. Hence, to describe these parts of the eigenfunctions, very high energy plane waves are needed, thereby greatly increasing computation time. A way around this problem is through the use of pseudopotentials.

3.4.1 Pseudopotentials versus all-electron methods

In the pseudopotential method, only the valence electrons are included explicitly as electrons in the calculation. The core electrons are taken into account only in an effective manner through their screening of the potential from the nuclei felt by the valence electrons. The screened effective potential – called the pseudopotential – no longer approaches negative infinity in regions close to the nuclei, removing the need for a large plane wave energy cutoff. Thus, computation time is greatly reduced in two ways: (1) a lower energy cutoff can be used, and (2) the number of electrons is smaller since the core electrons are not explicitly included. In general, the form of a pseudopotential of an atom is determined by requiring that the pseudo-eigenfunctions (obtained from solving Schrödinger's equation with the pseudopotential in place) match the true eigenfunctions for radial distances beyond some cutoff. For a given DFT implementation, there are typically several pseudopotentials available for each element differing in the number of electrons placed in the core.

Pseudopotential methods are particularly useful when studying properties which are dictated by the valence electrons. This is actually not too severe of a restriction since it is the valence orbitals, both occupied or unoccupied, which determine important aspects such as the low energy response to applied electromagnetic fields (i.e. all forms of spectroscopy) and chemical reactivity. In this work, since we deal with very large supercells of the LAO/STO heterojunction, it is computationally prohibitive to use all-electron methods. Therefore, we employ the pseudopotential method for all our calculations.

Chapter 4

Calculations and Results

4.1 Method

All DFT calculations reported in this thesis are performed with the Vienna *ab initio* simulation package (VASP) [42] using the projector augmented plane wave method [43, 44]. The PBE functional is used for the exchange-correlation energy. The energy cutoff for the plane-wave basis functions is 400 eV. For structural optimization calculations, a Γ-centered (7,7,1) k-point mesh is used. For density of states (DOS) calculations on the optimized structures, a Γ-centered (17,17,1) k-point mesh is used.

The structures simulated are comprised of m unit layers of LAO on top of 4 unit layers of STO substrate. The interface is n-type (TiO_2/LaO). K atoms are adsorbed on the surface AlO_2 layer of LAO at a concentration of 1 adsorbed atom per 2 lateral AlO_2 unit cells, *i.e.* the concentration needed for exact compensation of the polar problem. We refer to this as $K_{ads}(LAO)_m(STO)_4$. Coverages of 3 K per 4 lateral unit cells and 1 K per lateral unit cell are also considered. The $m = 2$ structure is shown in Fig. 4.1(a). We placed the K atoms above the center of squares formed by the oxygen atoms in the surface AlO_2 layer, as shown in Fig. 4.1(b). This position should be the most stable configuration because a K^+ cation is attracted to each O^{2-} anion. Indeed, alternate positions were found to be unstable towards relaxing back into this position, thus validating our choice.

The lateral lattice constant is fixed at $\sqrt{2}a$, where $a = 3.913$ Å is the calculated DFT-PBE lattice constant for bulk STO. Atoms of the bottom-most STO unit layer are kept fixed so as to simulate the effect of the infinitely thick substrate. All other atoms are allowed to relax along the z-direction until the force on each atom is less than 0.02 eV/Å. 15 Å of vacuum is placed above each slab to minimize interactions between periodic copies of the slab. Dipole corrections to the total energy and electric potential are used to remove any remaining spurious contributions due to periodic boundary conditions [45].

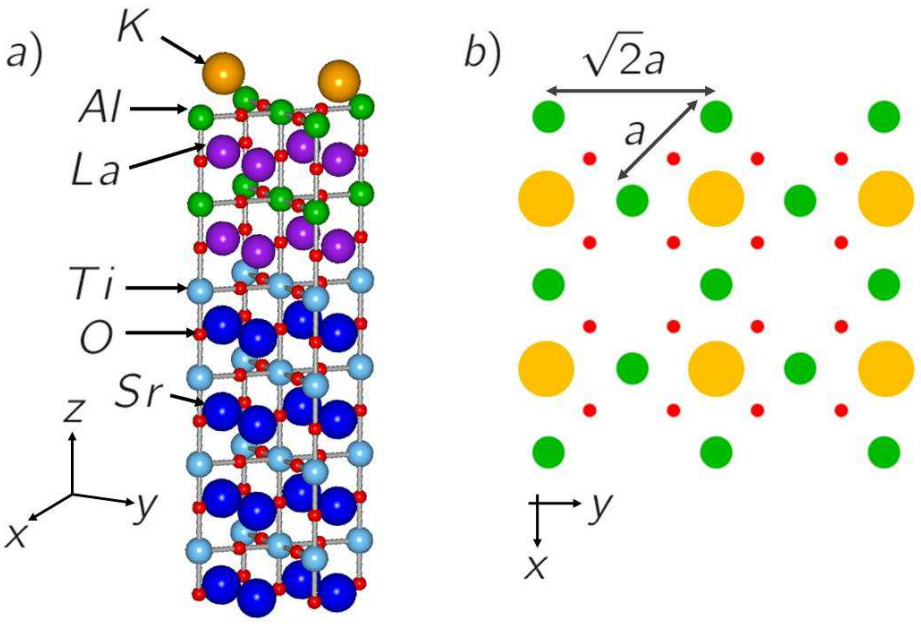

Figure 4.1: (a) $K_{ads}(LAO)_m(STO)_4$ for $m = 2$ (initial structure). K atoms are placed on the surface AlO_2 layer in the middle of the squares formed by oxygen atoms. This is illustrated in panel (b) which shows a top view of the K adsorption sites on the surface AlO_2 layer. The simulated square unit cell has a side length of $\sqrt{2}a$, where $a = 3.913$ Å is the lattice constant of bulk STO obtained from DFT.

4.2 Compensation by potassium electron donation

Layer and element projected partial densities of states (PDOS) are shown in Fig. 4.2(a) for $m = 3$. Upon K adsorption, electrons are donated into the Ti $3d$ conduction bands. The electron density is greatest for the titanate layer near the interface and decays for layers further away, forming a q-2DEG as in pure electronic reconstruction. In both cases, the extent of the electron transfer is limited by an associated energy cost. For pure electronic reconstruction, this is the band gap between the valence band of LAO and the conduction band of STO. In the present case, this is the binding energy of the $4s$ electron of the adsorbed K. This parameter controls how much of the diverging potential across LAO is compensated. To evaluate their efficiency, we look for residual potential buildup across the LAO film.

If $V(x, y, z)$ is the electric potential function, then the planar-average potential along z, $\bar{V}(z)$, is defined by:

$$\bar{V}(z) = \frac{1}{S} \int_S dxdyV(x, y, z), \tag{4.1}$$

where S is area of the lateral unit cell. It is also useful to define the macroscopic average potential, $\bar{\bar{V}}(z)$ [46]:

$$\bar{\bar{V}}(z) = \frac{1}{a_z} \int_{z-a_z/2}^{z+a_z/2} dz'\bar{V}(z'). \tag{4.2}$$

Here, a_z refers to the lattice constant of LAO in the z-direction. In other words, $\bar{\bar{V}}(z)$ averages out oscillations within one unit cell. Because of relaxation, especially in the uncompensated film, a constant a_z is actually ill-defined. For convenience, we take as a_z the relaxed thickness of LAO divided by the number of unit cells. One can also generalize the notion of the macroscopic average to account for the interface with STO [46], but since we are only interested in the potential buildup across LAO, we use the definition in Eq. 4.2.

In Fig. 4.2b, we plot $\bar{V}(z)$ and $\bar{\bar{V}}(z)$ within the LAO region for the system without adsorbed K. The same is shown for the system with adsorbed K in Fig. 4.2c. No potential buildup is observed across LAO in the system with K, whereas a potential buildup of ~ 2 eV is present in the system without K. This is evident looking at the overall slopes in the macroscopic potentials, as well as the positions of the minima in the planar-average potentials.

In an effort to explain why no residual potential is actually observed experimentally, Ref. [47] simulated the placement of metallic overlayers on

top of LAO/STO *after growth*; this has subsequently been done with Co [48]. The main conclusion was that the presence of metallic contacts used for measurements explains why residual potential is absent in experiment. One might extend these results of Ref. [47] as another way to remove the potential buildup. However, in this case the top layer is metallic and separating its conductivity from that of the q-2DEG is difficult. This is not an issue for our proposal, where the K surfactant layer is insulating after donating its electrons to the interface. Moreover, since the metal capping is done after growth, the tendency for defects and vacancies to form during growth is not mitigated. In contrast, as we argue below, the crystal grows underneath the K surfactant layer free of such defects.

It has been shown that in the absence of oxygen vacancies or other defects, the onset of electronic reconstruction is delayed through formation of polar distortions within the LaO layers, which create internal compensating dipoles that screen the electric potential. Below a critical thickness of 4-5 unit LAO layers, this suffices to partially compensate the polar potential. In thicker films with larger potential buildup, the compensation requires electronic reconstruction, which in turn removes the need for these polar distortions. It is thus worthwhile to consider whether a critical thickness, for similar reasons, exists for the transfer of the K $4s$ electron to the Ti $3d$ bands.

Fig. 4.3 shows DOS for $1 \leq m \leq 6$, with and without adsorbed K. The critical thickness at which the system without K becomes conducting is found to be of 4 LAO unit layers (Fig. 4.3(d)). In contrast, the system with adsorbed K is conducting for all thicknesses: even at one unit layer of LAO, where the potential across the film is smallest, K gives up its $4s$ electron to the Ti $3d$ bands and the polar distortions within LAO are eliminated.

4.3 Cohesive energies

Figures 4.2 and 4.3 show that K adsorption negates the polar catastrophe and stabilizes the LAO/STO heterojunction. The energetic stability can be quantified by calculating the cohesive energy $E_{coh}(m)$:

$$E_{coh}(m) = E_{K_{ads}LAO_mSTO_4} - E_{LAO_mSTO_4} - E_K, \tag{4.3}$$

where m is the number of unit layers of LAO, $E_{K_{ads}LAO_mSTO_4}$ is the total energy of the system with K adsorption, $E_{LAO_mSTO_4}$ is the total energy of the system without K adsorption (using the same size of lateral unit cell), and E_K is the energy per atom of metallic K (body-centered cubic). Thus

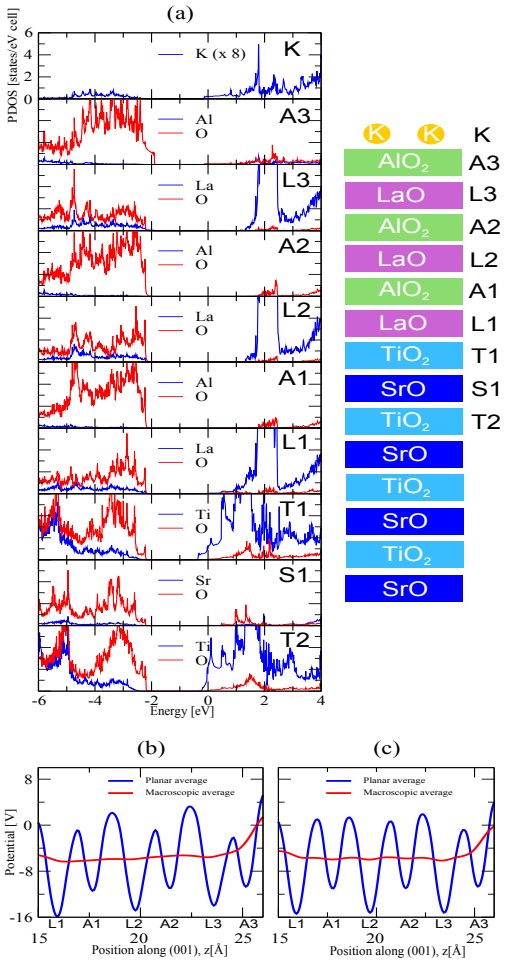

Figure 4.2: (a) Layer and element projected DOS for $K_{ads}(LAO)_3(STO)_4$. The Fermi energy is at 0. The scale is the same for all panels. Upon adsorption of K, the TiO_2 layers become conducting. The conduction electron density is greatest for the TiO_2 layer closest to the interface. The xy-planar-average and macroscopic average electric potentials are plotted versus the z-position along the (001) direction of the supercell, within the LAO region, for the system (b) without and (c) with K. A potential buildup of the order of 2 eV exists for the bare system without K. This is eliminated in the system with the K surfactant.

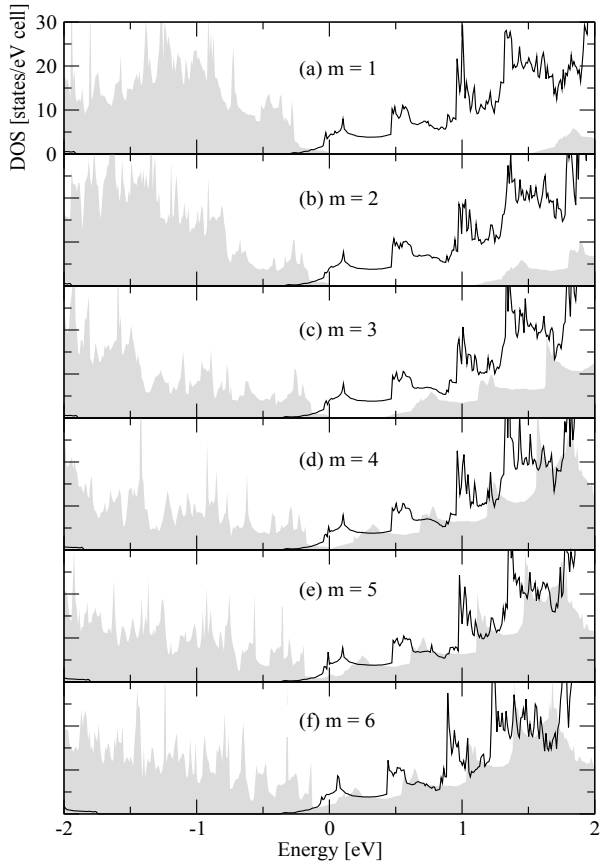

Figure 4.3: Total DOS for $(LAO)_m(STO)_4$, $m = 1 - 6$, with (black line) and without (shaded gray) K adsorption. The Fermi energy is at 0. The scale is the same for all panels. The critical thickness at which the system without K undergoes electronic reconstruction and becomes conducting is 4 unit layers of LAO. In contrast, the system with K is conducting at all LAO thicknesses simulated.

E_{coh} is the cohesive energy per adsorbed K with respect to metallic K. It is plotted as a function of m in Fig. 4.4.

Two observations can be made: (1) The K-adsorbed system becomes more stable relative to the original system as the number of LAO unit layers is increased. This is a trivial consequence of the potential buildup across LAO increasing with m—the greater the potential buildup, the greater the

energy reduction when it is eliminated by electron transfer from adsorbed K; (2) For the thicknesses considered, $|E_{coh}|$ ranges from 1 eV to over 2 eV, a very substantial energetic stabilization.

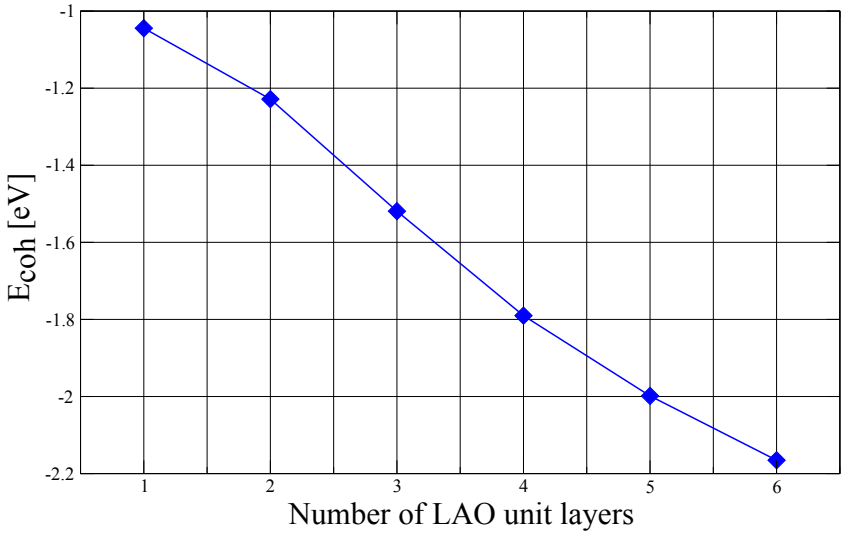

Figure 4.4: Cohesive energy per adsorbed K, defined in Eq. (4.3), as a function of the thickness of LAO. The system with K becomes more stable as the thickness increases. The cohesive energy is approximately 1 eV for 1 unit layer of LAO, increasing to more than 2 eV as LAO thickness is increased.

4.4 Potassium coverage beyond 1/2 per unit cell

We can also consider what happens if more potassium is adsorbed than the minimum of 1/2 per unit cell needed for compensation of the polar problem. In Figs. 4.5, we plot the K projected densities of states (PDOS) near E_F at three values of K coverage: 1/2 per unit cell, as well as 3/4 and 1 per unit cell. The thickness of the LAO layer is $m = 2$.

For the latter two coverages, Fig. 4.5 shows that although the K overlayer now has sufficient electrons to transfer more than 1/2 electron per unit

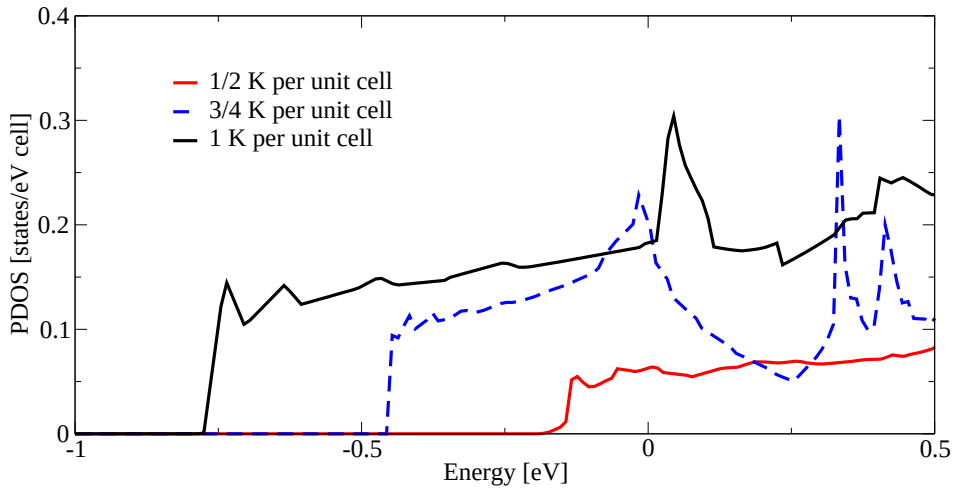

Figure 4.5: K PDOS near the Fermi energy, at three cases of K coverage, for LAO thickness of two unit layers. The density of conduction electrons retained by K increases significantly going from 1/2 to 3/4 per unit cell coverage, and then from 3/4 to 1 per unit cell coverage. Hence, K adsorption beyond the critical amount needed for the ideal exact compensation does not result in extra electrons being transferred to the interface; the extra electrons remain in the K overlayer.

cell to the interface, the extra electrons are retained in the K overlayer for the higher coverages beyond 1/2 K per unit cell, as expected. This indicates that K donates just enough electrons to compensate for the diverging potential. Anything beyond that would result in energetically expensive overcompensation.

The energetic favorability for further K adsorption can be quantified by calculating the additional cohesive energy upon adsorption of extra K atoms. In particular, we take as a reference 4 lateral unit cells of LAO/STO with 2 adsorbed K atoms (1/2 K per unit cell coverage), whose total energy we denote by $E_{K_2[LAO_2STO_4]_4}$. We can now further adsorb 1 or 2 more K atoms onto this system to attain 3/4 and 1 per unit cell K coverage. We denote the total energies of these systems by $E_{K_3[LAO_2STO_4]_4}$ and $E_{K_4[LAO_2STO_4]_4}$, respectively. The extra cohesive energies upon adsorption of each additional K can then be defined as:

$$E_{coh,3/4} = E_{K_3[LAO_2STO_4]_4} - E_{K_2[LAO_2STO_4]_4} - E_K, \tag{4.4}$$

$$E_{coh,4/4} = E_{K_4[LAO_2STO_4]_4} - E_{K_3[LAO_2STO_4]_4} - E_K. \tag{4.5}$$

We find that $|E_{coh,3/4}| = 0.39$ eV and $|E_{coh,4/4}| = 0.56$ eV. These are to be contrasted with the cohesive energy per adsorbed K for the first two adsorbed K atoms, which was calculated to be 1.2 eV (Fig. 4.4). The cohesive energy as defined is approximately 0.7-0.8 eV smaller for K atoms adsorbed beyond the critical 1/2 per unit cell coverage, *i.e.* it is much less energetically favorable for extra K atoms to be adsorbed onto the system. This observation is critical for preventing any undesired accumulation of K onto the surface. In particular, the large cohesive energy difference between K atoms adsorbed up to 1/2 coverage and K atoms adsorbed beyond 1/2 coverage suggests that if the substrate temperature is kept higher than some critical threshold, then any extra K will evaporate off. This would prevent a thick layer of K metal from forming on the surface and hence fundamentally changing the system—the surfactant density will stabilize at exactly the density needed to compensate for the diverging potential.

4.5 Undesired substitutions of K into LAO

Our proposal to use a K surfactant to stabilize the epitaxial growth of LAO/STO(001) hinges on K remaining on the AlO_2 surface instead of entering into LAO by substitution of La or Al ions. Substitution is highly unlikely given the large differences in ionic radii between K^+ (151 pm), La^{3+} (116 pm) and Al^{3+} (54 pm) [49]. We confirm this by calculating the total energy change if K exchanges position with an La or Al ion close to the surface, in a $m = 5$ film (results are expected to be representative for all m).

Consider first the exchange of K with a La ion in the top LaO layer. The energy cost per substituted K is 1.93 eV if K exchanges positions with the La beneath it, and 2.27 eV for the other La (*cf.* Fig. 4.1). In a striking display of how energetically unfavorable is the substitution of K for Al, our relaxation of the substituted structure resulted in the K pushing its way back above the rest of the structure. Substitution into deeper layers of LaO/AlO_2 is expected to be just as, if not more, energetically costly. This proves that the energy cost for K substitution of La/Al within the bulk of LAO is indeed very large.

Chapter 5

Summary and Conclusions

To summarize, we have shown that K adsorbed on the AlO_2 surface of an n-type LAO/STO(001) heterojunction compensates the diverging electric potential across LAO by donating its $4s$ electron to the Ti $3d$ conduction band. The compensation is highly efficient, with very little residual potential buildup across LAO. Also, substitution of K into layers of LAO by exchange with La or Al is demonstrated to be extremely unfavorable.

Taken together, these results suggest an elegant scheme for growing clean LAO/STO heterojunctions and polar films in general. By executing the growth in the presence of alkali metals with low ionization energies, the diverging potential is eliminated without appealing to the myriad of other – often uncontrollable – compensation mechanisms. On a practical level, this requires only a small surface concentration of K, of $\sim 10^{14}/\text{cm}^2$. The cohesive energy for K adsorbed beyond the 1/2 per unit cell (ideal) concentration is significantly smaller than for the ideal concentration. Hence, if the substrate temperature is sufficiently high, any extra K will evaporate, preventing the formation of an undesired thick metallic overlayer of K on the surface. The large size of K also prevents the alkali metal cations from being incorporated into the film during growth, guaranteeing their role as surfactants. In constrast, smaller $3d$ transition metal ions (TM) would not be suitable because most of them form $LaTMO_3$ perovskite structures with similar lattice constants as LAO so it is reasonable to expect that they would substitute for Al during growth.

In principle, it is possible that K may undergo oxidation with the resulting oxide accumulating on the surface, impeding further growth. Whether this really happens can only be ascertained through experiment. If it does, a potential solution is to grow the first two or three layers without K, allowing the internal buckling to compensate for the potential buildup [25]. The O, La, and Al sources are then shut off, after which K is absorbed onto the exposed AlO_2 surface. This will remove the buckling since the K will take over in compensating for the polar problem. The K source is then turned off and the growth of the LAO is restarted, with the film growing cleanly underneath the layer of K surfactant.

Most importantly, our proposal can become a new paradigm for growing LAO/STO(001) samples that no longer have properties highly sensitive to growth conditions. The problem of electronic and structural properties being attributed to different defects in samples prepared differently has been identified as a major potential pitfall for the development of applications based on the LAO/STO interface [9]. We believe that the method proposed here solves this problem not just for LAO/STO, but for many systems in which clean growth in a particular direction is impeded by the polar catastrophe.

Bibliography

[1] A. Ohtomo and H. Hwang, Nature **427**, 423 (2004).

[2] S. Thiel, G. Hammerl, A. Schmehl, C. Schneider, and J. Mannhart, Science **313**, 1942 (2006).

[3] N. Nakagawa, H. Y. Hwang, and D. A. Muller, Nature Mater. **5**, 204 (2006).

[4] A. Savoia, D. Paparo, P. Perna, Z. Ristic, M. Salluzzo, F. Miletto Granozio, U. Scotti di Uccio, C. Richter, S. Thiel, J. Mannhart, and L. Marrucci, Phys. Rev. B **80**, 075110 (2009).

[5] N. Reyren, S. Thiel, A. D. Caviglia, L. F. Kourkoutis, G. Hammerl, C. Richter, C. W. Schneider, T. Kopp, A.-S. Rüetschi, D. Jaccard, *et al.*, Science **317**, 1196 (2007).

[6] N. Pavlenko, T. Kopp, E. Y. Tsymbal, G. A. Sawatzky, and J. Mannhart, Phys. Rev. B **85**, 020407 (2012).

[7] D. A. Dikin, M. Mehta, C. W. Bark, C. M. Folkman, C. B. Eom, and V. Chandrasekhar, Phys. Rev. Lett. **107**, 056802 (2011).

[8] C. Cen, S. Thiel, G. Hammerl, C. Schneider, K. Andersen, C. Hellberg, J. Mannhart, and J. Levy, Nature Mater. **7**, 298 (2008).

[9] J. Mannhart and D. G. Schlom, Science **327**, 1607 (2010).

[10] R. Hesper, L. H. Tjeng, A. Heeres, and G. A. Sawatzky, Phys. Rev. B **62**, 16046 (2000).

[11] A. S. Kalabukhov, Y. A. Boikov, I. T. Serenkov, V. I. Sakharov, V. N. Popok, R. Gunnarsson, J. Börjesson, N. Ljustina, E. Olsson, D. Winkler, and T. Claeson, Phys. Rev. Lett. **103**, 146101 (2009).

[12] L. Yu and A. Zunger, arXiv:1402.0895 .

[13] B. G. Levi, Phys. Today **60**, 23 (2007).

[14] J. N. Eckstein, Nature Mater. **6**, 473 (2007).

[15] W. Siemons, G. Koster, H. Yamamoto, W. A. Harrison, G. Lucovsky, T. H. Geballe, D. H. A. Blank, and M. R. Beasley, Phys. Rev. Lett. **98**, 196802 (2007).

[16] S. Pauli and P. Willmott, J. Phys.: Condens. Matter **20**, 264012 (2008).

[17] N. Pavlenko, T. Kopp, E. Y. Tsymbal, J. Mannhart, and G. A. Sawatzky, Phys. Rev. B **86**, 064431 (2012).

[18] L. Zhang, X.-F. Zhou, H.-T. Wang, J.-J. Xu, J. Li, E. G. Wang, and S.-H. Wei, Phys. Rev. B **82**, 125412 (2010).

[19] N. C. Bristowe, P. B. Littlewood, and E. Artacho, Phys. Rev. B **83**, 205405 (2011).

[20] Z. Zhong, P. X. Xu, and P. J. Kelly, Phys. Rev. B **82**, 165127 (2010).

[21] H. Chen, A. Kolpak, and S. Ismail-Beigi, Phys. Rev. B **82**, 085430 (2010).

[22] Y. Li, S. N. Phattalung, S. Limpijumnong, J. Kim, and J. Yu, Phys. Rev. B **84**, 245307 (2011).

[23] E. Slooten, Z. Zhong, H. J. A. Molegraaf, P. D. Eerkes, S. de Jong, F. Massee, E. van Heumen, M. K. Kruize, S. Wenderich, J. E. Kleibeuker, M. Gorgoi, H. Hilgenkamp, A. Brinkman, M. Huijben, G. Rijnders, D. H. A. Blank, G. Koster, P. J. Kelly, and M. S. Golden, Phys. Rev. B **87**, 085128 (2013).

[24] J. Zhou, T. C. Asmara, M. Yang, G. A. Sawatzky, Y. P. Feng, and A. Rusydi, (unpublished).

[25] R. Pentcheva and W. E. Pickett, Phys. Rev. Lett. **102**, 107602 (2009).

[26] V. Vonk, M. Huijben, K. J. I. Driessen, P. Tinnemans, A. Brinkman, S. Harkema, and H. Graafsma, Phys. Rev. B **75**, 235417 (2007).

[27] E. Tournié and K. H. Ploog, Thin Solid Films **231**, 43 (1993).

[28] D. Kandel and E. Kaxiras, arXiv:cond-mat/9901177 .

[29] E. Kaxiras, Mater. Sci. Eng., B **30**, 175 (1995).

[30] K. Mae, K. Kyuno, and R. Yamamoto, Modelling Simul. Mater. Sci. Eng. **4**, 73 (1996).

[31] R. Cao, X. Yang, J. Terry, and P. Pianetta, Appl. Phys. Lett. **61**, 2347 (1992).

[32] M. Copel, M. C. Reuter, E. Kaxiras, and R. M. Tromp, Phys. Rev. Lett. **63**, 632 (1989).

[33] H. H. Heikens, C. F. V. Bruggen, and C. Haas, Jpn. J. Appl. Phys. **19**, 399 (1980).

[34] S. Tixier, M. Adamcyk, E. Young, J. Schmid, and T. Tiedje, J. Cryst. Growth **251**, 449 (2003).

[35] E. Young, S. Tixier, and T. Tiedje, J. Cryst. Growth **279**, 316 (2005).

[36] D. Fournier, G. Levy, Y. Pennec, J. L. McChesney, A. Bostwick, E. Rotenberg, R. Liang, W. N. Hardy, D. A. Bonn, I. S. Elfimov, and A. Damascelli, Nature Phys. **6**, 905 (2010).

[37] M. A. Hossain, J. D. F. Mottershead, D. Fournier, A. Bostwick, J. L. McChesney, E. Rotenberg, R. Liang, W. N. Hardy, G. A. Sawatzky, I. S. Elfimov, D. Bonn, and A. Damascelli, Nature Phys. **4**, 527 (2008).

[38] P. Hohenberg and W. Kohn, Phys. Rev. **136**, B864 (1964).

[39] W. Kohn and L. J. Sham, Phys. Rev. **140**, A1133 (1965).

[40] J. P. Perdew and Y. Wang, Phys. Rev. B **45**, 13244 (1992).

[41] J. P. Perdew, K. Burke, and M. Ernzerhof, Phys. Rev. Lett. **77**, 3865 (1996).

[42] G. Kresse and J. Furthmüller, Phys. Rev. B **54**, 11169 (1996).

[43] P. E. Blöchl, Phys. Rev. B **50**, 17953 (1994).

[44] G. Kresse and D. Joubert, Phys. Rev. B **59**, 1758 (1999).

[45] G. Makov and M. C. Payne, Phys. Rev. B **51**, 4014 (1995).

[46] M. Peressi, N. Binggeli, and A. Baldereschi, J. Phys. D: Appl. Phys. **31**, 1273 (1998).

[47] R. Arras, V. G. Ruiz, W. E. Pickett, and R. Pentcheva, Phys. Rev. B **85**, 125404 (2012).

[48] E. Lesne, N. Reyren, D. Doennig, R. Mattana, H. Jaffrès, V. Cros, F. Petroff, F. Choueikani, P. Ohresser, R. Pentcheva, *et al.*, Nat. Commun. **5** (2014).

[49] W. Haynes, *CRC Handbook of Chemistry and Physics, 93rd Edition*, CRC Handbook of Chemistry and Physics (Taylor & Francis, 2012) .